JOURNAL OF AIRCRAFT
Vol. 47, No. 5, September–October 2010

Dynamic Stability Analysis of a Tethered Aerostat

Ashok Rajani,* Rajkumar S. Pant,† and K. Sudhakar‡
Indian Institute of Technology, Bombay, Mumbai 400 076, India

DOI: 10.2514/1.47010

This paper describes a model that has been developed to study the stability characteristics of aerostats. This model incorporates the concepts of apparent mass, dynamic tether and allows 6 degrees of freedom for the motion of the aerostat. Estimation of aerodynamic coefficients is based on empirical relations and curves available in literature. Weight and buoyancy are calculated based on geometry of the aerostat. Appropriate values for operational altitude and desired angle of attack of the aerostat are assumed. Moment balance about confluence point gives the optimal location of the confluence point. Equations of motion for the aerostat and dynamic tether are simulated and appropriate boundary conditions are applied. Force balance gives the tether tension force and its orientation at the confluence point. Based on the tether tension and its orientation at the confluence point, the tether profile is estimated by breaking up the tether into several elastic segments, each in equilibrium. Once equilibrium is established, the wind is perturbed and the response of the aerostat is simulated. The paper reports the results of simulation carried out for the TCOM 365Y aerostat and the aerostat response to various ambient velocity profiles.

I. Introduction

TETHERED aerostats fall under the category of lighter-than-air systems. A gas having lower density compared with ambient air (usually hydrogen or helium) is enclosed in an envelope and the difference in their densities gives rise to buoyancy. In an aerostat, buoyancy is the major source of lift, whereas in heavier-than-air systems (e.g., fixed-wing aircraft or rotorcraft), aerodynamic lift produced due to relative motion between the ambient air and the vehicle is the major source of lift. The various components of a typical aerostat system are outlined in Fig. 1.

The hull or envelope is a bag containing the lifting gas. Fins are attached at the rear end of the hull and provide stability to the aerostat; they are usually in the form inflated structures, filled with lifting gas or air. The payload, which is usually a surveillance camera or a radar, is mounted one the envelope. A series of ropes called confluence lines connect the hull to a single point called confluence point, to which the main tether is attached.

Aerostats can remain stationary for long duration in reasonable weather, which makes them a very good choice for surveillance, advertising, and raising antennae for wireless communication, to name a few. In real life, aerostats have to operate in highly varying weather conditions and winds. Aerostat failures have occurred because of abrupt changes in the wind, which result in shock loads. Estimation of these shock loads is an important requirement in aerostat design, and it can be accomplished by modelling the dynamics of an aerostat and predicting its response to sharply fluctuating winds.

This paper starts with a brief history on the development of modeling and simulation of aerostats. The next section deals with equilibrium analysis of tethered aerostats, in which the angle of attack α at which the aerostat is in equilibrium as a function of ambient wind speed U is determined. Aerodynamic coefficients need to be estimated for equilibrium analysis, which can be done using empirical relations based on the aerostat geometry, as explained in the next section. The next section gives details of the simulation model that was developed for simulating the response of aerostat. The results obtained by running the analysis for the TCOM 365Y aerostat are presented next. The aerodynamic and geometric parameters are compared with those from literature. The conclusions drawn from the results and also scope for future work are presented in the last section.

II. Historical Development of Modeling and Simulation of Aerostats

Information related to stability analysis of aerostats in open literature is quite sparse, as the work has mostly been done by private organizations, e.g., TCOM. First-order stability analysis of an aerodynamically shaped tethered balloon was reported by DeLaurier [1], which was extended by him to predict RMS lateral response, using transfer functions [2]. Based on wind-tunnel data of five scaled models of aerostats, Jones and DeLaurier [3] developed empirical techniques for approximate the aerodynamics parameters in 1981. Using these formulae, Jones and Krausman [4] developed a 6-DOF nonlinear dynamic simulation model (NDLS) for obtaining the response of a tethered aerostat to turbulence and other disturbances, and validated it against experimental results. In this study a *frozen-field* turbulence model was used, in which a continuous turbulence spectrum is simulated by combining a number of discrete wavelengths in random phase, where the amplitudes are calculated through integration of the Dryden power density spectrum. The NDLS model was further improved and validated against full-scale fight tests of an instrumented TCOM 71M tethered aerostat by Jones and Schroeder [5].

Lambert and Nahon [6] have also presented a nonlinear model for investigating the dynamics of a tethered aerostat. However, they have linearized the system using a finite difference approach. They have presented results for several longitudinal and lateral modes, and have also considered the cross coupling between the tether and aerostat.

Stanney and Rahn [7] have used an improved atmospheric model, and validated the experimental results listed cited by Jones and Schroeder [5], using a nonlinear 2-D aerostat model, which includes a rigid body with aerodynamic loading attached to a continuous tether. They have also generated gust inputs using real hurricane data to predict the aerostat response to severe turbulences.

Surviving harsh weather conditions, especially in the presence of strong winds, is a major challenge in aerostat operation, particularly for those intented for long duration operations. Rawat [8] has carried out a simulation of tethered aerostats using nonlinear differential equations derived using the Lagrangian theory, on a lumped parameter model, without linearizing them. He has investigated three typical scenarios of aerostat-weather interactions, viz., effect of a

Received 11 September 2009; revision received 22 January 2010; accepted for publication 15 June 2010. Copyright © 2010 by Ashok Rajani, Rajkumar S. Pant, and K. Sudhakar. Published by the American Institute of Aeronautics and Astronautics, Inc., with permission. Copies of this paper may be made for personal or internal use, on condition that the copier pay the $10.00 per-copy fee to the Copyright Clearance Center, Inc., 222 Rosewood Drive, Danvers, MA 01923; include the code 0021-8669/10 and $10.00 in correspondence with the CCC.

*Undergraduate Student, Department of Aerospace Engineering.
†Associate Professor, Department of Aerospace Engineering. Member AIAA.
‡Professor, Department of Aerospace Engineering. Member AIAA.

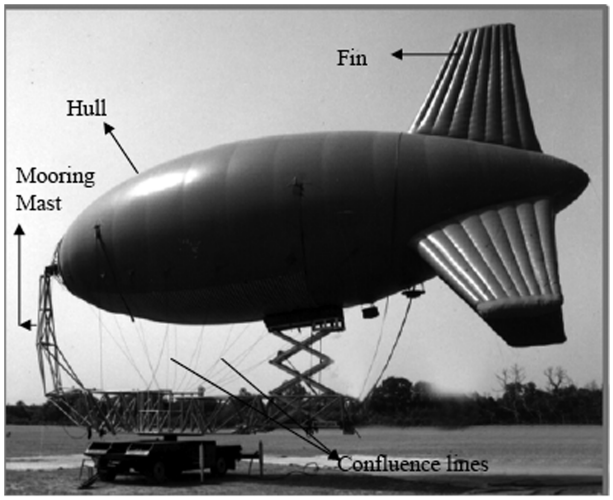

Fig. 1 A 250 m^3 aerostat developed by Aerial Delivery R & D Establishment in India [15].

passing downdraft on an aerostat, a gust during aerostat's recovery, and a lateral gust on a moored aerostat.

III. Equilibrium and Stability Analysis of Tethered Aerostats

Stability is defined for an equilibrium state. An equilibrium analysis for the aerostat needs to be carried out and then that equilibrium state needs to be analyzed for stability. The methodology for equilibrium analysis of tethered aerostats has been provided by Panda and Krishnamurthy [9], which is described in the following section.

A. Force and Moment Balance

The following forces and moments act on an aerostat: 1) weight acting about the center of mass, 2) buoyancy acting about the center of buoyancy, 3) aerodynamic forces acting about the center of pressure, that may be represented as forces and a constant moment acting at aerodynamic center, and 4) tether tension acting about the confluence point.

The coordinate system used for the equilibrium analysis is the body fixed system (BFS) with origin at the nose of the body, X axis pointing to the rear of the body along its axis of symmetry and the Z axis upward. The aerostat experiences steady horizontal winds at an angle of attack α as shown in Fig. 2.

Aerodynamic forces and moments act at x_a, buoyancy force acts at x_b, and the weight at x_g; all these points are assumed to be on the axis of symmetry. The confluence point is located at (x_c, z_c). Two distances $c_x = x_g - x_c$ and $c_z = z_g - z_c$ are defined.

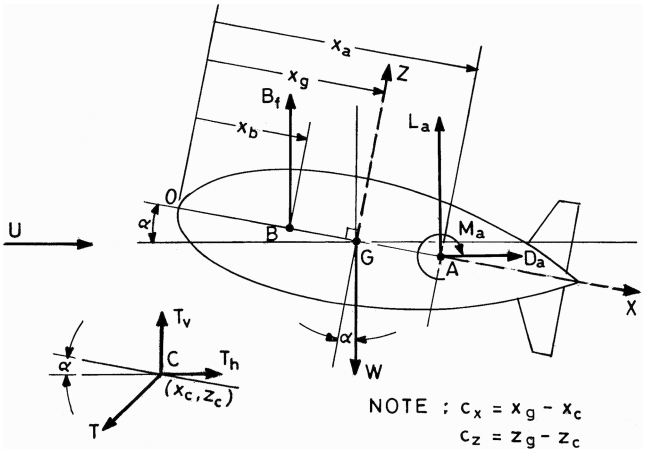

Fig. 2 Forces acting on a typical aerostat.

Balancing forces in the X-Z plane, we get the following equations:

$$F_{ax} - B_f \sin\alpha + W \sin\alpha + T_h \cos\alpha - T_v \sin\alpha = 0 \tag{1}$$

$$F_{az} + B_f \cos\alpha - W \cos\alpha + T_h \sin\alpha + T_v \cos\alpha = 0 \tag{2}$$

Balancing moments about the confluence point gives:

$$M_a - F_{az}(x_a - x_g + c_x) + (F_{ax} - B_f \sin\alpha + W \sin\alpha)c_z - B_f \cos\alpha(x_b - x_g + c_x) + c_x W \cos\alpha = 0 \tag{3}$$

where

$$F_{ax} = \frac{1}{2}\rho U^2 A[-C_L \sin\alpha + C_D \cos\alpha] \quad \text{and}$$
$$F_{az} = \frac{1}{2}\rho U^2 A[C_L \cos\alpha + C_D \sin\alpha] \tag{4}$$

$$M_a = \frac{1}{2}\rho U^2 A l C_{M0} \tag{5}$$

C_L and C_D in turn are given by

$$C_L = a_v \sin\alpha \qquad C_D = C_{D0} + K\alpha^2 \tag{6}$$

Let us define $\bar{c}_x$, $\bar{c}_z$, $\bar{x}_a$, $\bar{x}_g$, and $\bar{x}_b$ as distances nondimensionalized with the envelope length l.

Simplifications after substitution yields Eq. (7)

$$C_M = C_{M0} - \left[\frac{a_v}{2}\sin 2\alpha + C_D \sin\alpha\right](\bar{x}_a - \bar{x}_g + \bar{c}_x) + [-a_v \sin\alpha^2 + C_D \cos\alpha]\bar{c}_z] - \frac{B_f}{\frac{1}{2}\rho U^2 A}[\cos\alpha(\bar{x}_b - \bar{x}_g + \bar{c}_x) + \bar{c}_z \sin\alpha] + \frac{W}{\frac{1}{2}\rho U^2 A}[\bar{c}_x \cos\alpha + \bar{c}_z \sin\alpha] \tag{7}$$

For a given speed U, the angle of attack α adjusts itself to satisfy $C_M = 0$ and results in Eq. (8)

$$C_{M0} - (a_v \sin\alpha\cos\alpha + (C_{D0} + K\alpha^2)\sin\alpha)(\bar{x}_a - \bar{x}_g + \bar{c}_x) - (a_v \sin\alpha^2 - (C_{D0} + K\alpha^2)\cos\alpha)\bar{c}_z = \frac{1}{\frac{1}{2}\rho U^2 A}[B_f(\cos\alpha(\bar{x}_b - \bar{x}_g + \bar{c}_x) + \bar{c}_z \sin\alpha) - W(\bar{c}_x \cos\alpha + \bar{c}_z \sin\alpha)] \tag{8}$$

Using Eq. (8), it can be shown that the equilibrium angle of attack is maximum at $U = 0$; and as U increases, α decreases asymptotically to a value $\alpha_{\min}$.

B. Confluence Point

An appropriate choice of confluence point can make the equilibrium angle of attack independent of wind speed U [9]. This can be done by setting the left-hand side (LHS) and right-hand side (RHS) of Eq. (8) separately equal to 0. This will yield Eqs. (9) and (10) in terms of $\bar{c}_x$ and $\bar{c}_z$, respectively

$$\bar{c}_x = \frac{C_{M0}\sin\alpha}{C_{D0} + K\alpha^2} - \left(1 + \frac{a_v \cos\alpha}{C_{D0} + K\alpha^2}\right)\left[(\bar{x}_a - \bar{x}_g) + \frac{(\bar{x}_g - \bar{x}_b)}{1 - \frac{W}{B_f}}\right]\sin\alpha^2 + \frac{(\bar{x}_g - \bar{x}_b)}{1 - \frac{W}{B_f}} \tag{9}$$

$$\bar{c}_z = -\frac{C_{M0}\cos\alpha}{C_{D0} + K\alpha^2} + \left(1 + \frac{a_v \cos\alpha}{C_{D0} + K\alpha^2}\right)\left[(\bar{x}_a - \bar{x}_g) + \frac{(\bar{x}_g - \bar{x}_b)}{1 - \frac{W}{B_f}}\right]\sin\alpha\cos\alpha \tag{10}$$

C. Stability Margin

Static stability in pitch is characterized by $\frac{dC_M}{d\alpha}$, and can be easily shown to be

$$\frac{dC_M}{d\alpha} = \frac{W}{\frac{1}{2}\rho U^2 A}[\bar{c}_z \cos\alpha - \bar{c}_x \sin\alpha] + \frac{B_f}{\frac{1}{2}\rho U^2 A}[\sin\alpha(\bar{x}_b - \bar{x}_g + \bar{c}_x) - \bar{c}_z \cos\alpha] - [a_v \cos 2\alpha + C_D \cos\alpha + C_{D\alpha} \sin\alpha](\bar{x}_a - \bar{x}_g + \bar{c}_x) - [a_v \sin 2\alpha + C_D \sin\alpha - C_{D\alpha} \cos\alpha]\bar{c}_z \quad (11)$$

IV. Estimation of Aerodynamic Coefficients and Tether Profile

Aerodynamic coefficients are needed for estimating the aerodynamic forces acting on an aerostat under given wind conditions. A semi-empirical model for finned axisymmetric bodies was developed by Jones and DeLaurier [3], which was modified for unsymmetrically finned bodies by Gill et al. [10], details of which are outlined below.

A. Aerodynamic Forces and Moments

The normal force acting on the aerostat is [3]:

$$L = q_0((k_3 - k_1)\eta_k I_1 \sin(2\alpha)\cos(\alpha/2) + (Cd_c)_h \sin(\alpha)\sin(\alpha)J_1 + S_f[(C^\star_{n\alpha})_f \eta_f(\sin(2\alpha)/2) + (Cd_c)_f \sin(\alpha)\sin(\alpha)]) \quad (12)$$

The efficiency factors η_f and η_k account for mutual interference between hull and fins. Similarly, the axial or drag force is given by:

$$D = q_0[(Cd_h)_0 S_h + (Cd_f)_0 S_f]\cos\alpha^2 - (k_3 - k_1)\eta_k I_1 \sin(2\alpha)\sin(\alpha/2) - (C_t)_f S_f \quad (13)$$

The aerodynamic moment about nose is given by:

$$M_{\text{nose}} = -q_0[(k_3 - k_1)\eta_k I_3 \sin(2\alpha)\cos(\alpha/2) + (Cd_c)_h \sin(\alpha)\sin(\alpha)J_2 + S_f[\eta_f(l_f)_1(C^\star_{n\alpha})_f(\sin(2\alpha)/2) + (l_f)_2(Cd_c)_f \sin(\alpha)\sin(\alpha)]] \quad (14)$$

where

$$I_1 = \int_0^{l_h} \frac{dA}{d\zeta}\, d\zeta, \qquad I_3 = \int_0^{l_h} \zeta \frac{dA}{d\zeta}\, d\zeta$$
$$J_1 = \int_0^{l_h} 2r\, d\zeta \quad \text{and} \quad J_2 = \int_0^{l_h} 2r\zeta\, d\zeta \quad (15)$$

The above expressions for aerodynamic forces and moments assume the resultant forces to be acting at the nose of the hull. The forces and integrals are nondimensionalized with respect to S_{ref}, defined as Volume$^{2/3}$ and the moment is nondimensionalized with $S_{\text{ref}} l_h$.

B. Estimation of Coefficients

1. Fin Lift Curve Slope $C^\star_{n\alpha}$

$C^\star_{n\alpha}$ can be estimated using the formula given in Raymer [11]

$$C^\star_{n\alpha} = \frac{2\pi \text{AR}}{2 + \sqrt{4 + \frac{\text{AR}^2}{\beta^2\eta^2}(1 + \tan(\Lambda_{\frac{1}{2}c}))}} \quad (16)$$

This formula is valid for zero dihedral angle. If the fin has a dihedral, the projected area changes and so does the angle of attack; both diminish by a factor of $\cos(\Gamma)$.

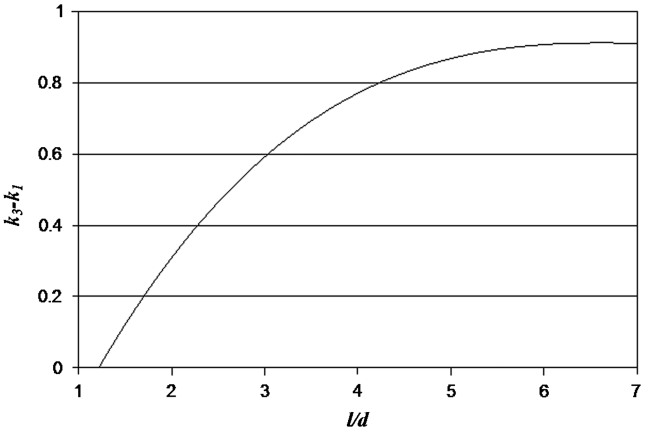

Fig. 3 Lateral and axial apparent mass coefficient difference [12].

2. Apparent Mass Coefficient ($k_3 - k_1$)

The variation of the apparent mass coefficient with l/d was estimated from Munk [12]. A six-degree polynomial was fitted to the data, and the graph is reproduced here as Fig. 3.

3. Hull and Fin Zero Angle Cross Flow Drag Coefficient

$$(Cd)_0 = (Cd)_{\text{wet}} \frac{S_{\text{wet}}}{S_{\text{ref}}} C_f \quad (17)$$

where

$$(Cd_h)_{\text{wet}} = 1 + \frac{3}{2}\left(\frac{l}{d}\right)^{\frac{-3}{2}} + 7\left(\frac{l}{d}\right)^{-}3 \quad \text{and}$$
$$(Cd_f)_{\text{wet}} = 1 + \frac{6}{5}\left(\frac{t}{c}\right) + 100\left(\frac{t}{c}\right)^4 \quad (18)$$

C_f as a function of Reynolds number is given by [13]

$$C_f = K/R_l^{1/3} \quad (19)$$

For $10^6 < R_l < 10^8$, $m = 6$ and $k = 0.44$ is a good approximation, whereas for $10^7 < R_l < 10^9$, $m = 7$ and $k = 0.03$. Here R_l is the Reynolds number.

4. Fin and Hull Cross Flow Drag Coefficient $(Cd_c)_f$

For operating conditions of airships, $(Cd_c)_h$ is an independent parameter, and its value is taken as 0.32 [13].

A graph for the variation of $(Cd_c)_f$ with aspect ratio and taper ratio is provided by Gill et al. [10] and is reproduced in Fig. 4.

5. Fin and Hull Efficiency Factors

The curves for η_f and η_k are as given in Fig. 5. Curve fitting was done to eliminate the need for manual entries of these coefficients. η_f was approximated by a 6 ° polynomial, whereas a 3 ° polynomial was used to approximate eta_k.

C. Computation of Mass Matrix

The mass matrix is composed of two components, the real mass matrix and the apparent mass matrix [A], which is a 6×6 diagonal matrix. The magnitude of this apparent mass depends on the dimensions of the body. The ratio of apparent mass to the actual mass of the body is quite significant for an aerostat and hence must be incorporated in the model of an aerostat. Both the matrices were evaluated using the formulae listed in ACT.[§]

[§]Aircraft Control Toolbox (ACT) is a software for use with MATLAB®.

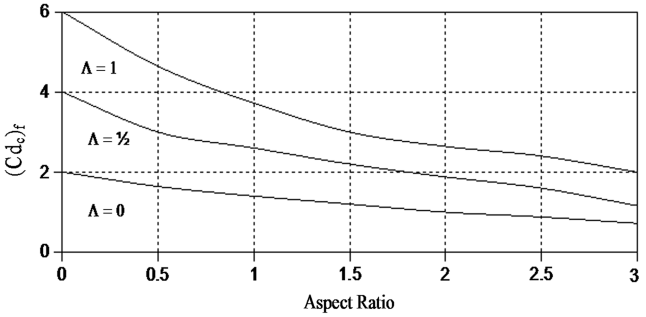

Fig. 4 Fin crossflow drag coefficient [16].

1. Apparent Mass Matrix

The components of the apparent mass matrix A are given by:

$$A(1,1) = \frac{-\alpha \times \text{mass}}{2-\alpha} \tag{20}$$

$$A(2,2) = A(3,3) = \frac{-\beta \times \text{mass}}{2-\beta} \tag{21}$$

$$A(5,5) = A(6,6) = -\frac{0.2\,\text{mass}\,bA^2}{2bA + (b^2+a^2)(\beta-\alpha)} \tag{22}$$

The remaining terms of A are all zero.

2. Real Mass Matrix

The elements of real mass matrix R are given by:

$$R(1,1) = R(2,2) = R(3,3) = M_{\text{total}} \tag{23}$$

where M_{total} is the total mass of the aerostat.

The remaining diagonal terms are the moments of inertia

$$R(4,4) = I_{xx} \qquad R(5,5) = I_{yy} \qquad R(6,6) = I_{zz} \tag{24}$$

Because the aerostat is a body of revolution, the products of inertia are zero

$$R(i,j) = 0 \qquad i \neq j \tag{25}$$

The mass matrix is now given by:

$$[M] = [R] + [A] \tag{26}$$

D. Tether Profile Estimation

The tether profile depends on the tension acting at the confluence point and the aerodynamic forces acting on it. The tether is divided into many straight elastic segments which are connected by nodes. Each segment is modeled as a spring–mass–dashpot system with segmental mass assumed to be concentrated at the nodes. The forces acting on each element of the tether are depicted in Fig. 6.

Each segment is acted upon by three forces: tension forces from segments before and after it, aerodynamic drag acting on that segment, and weight of that segment. For estimation of drag forces, the tether is assumed to be a cylinder. C_D for cylinder with flow normal to its axis is much higher than the C_D for flow along the axis. Thus, the drag force is assumed to act normal to the axis of the cylinder as depicted in Fig. 6.

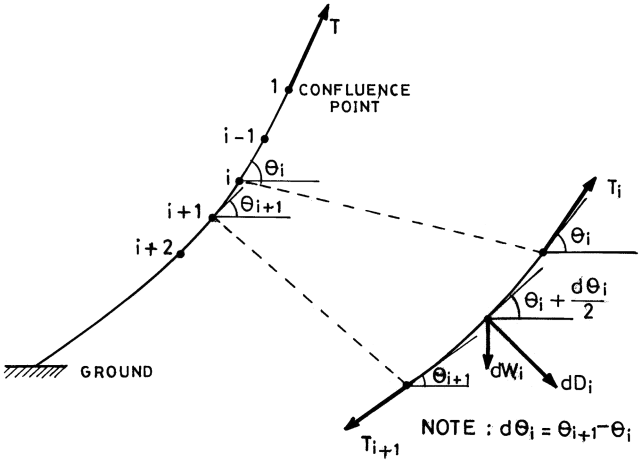

Fig. 6 Forces acting on each element of tether.

Let $\theta(i)$ be the angle that the ith segment makes with the horizontal and let $T(i)$ be the tension force acting on it. Balancing forces along the X and Z axes, we get:

$$T(i)\cos\theta(i) + dD\sin\theta(i) = T(i+1)\cos\theta(i+1) \tag{27}$$

$$T(i)\sin\theta(i) = dD\cos\theta(i) + dW(i) + T(i+1)\sin\theta(i+1) \tag{28}$$

where

$$dW(i) = \rho_t dS(i) \quad \text{and} \quad dD(i) = \frac{1}{2}\rho[V\sin(\theta(i))]^2 dS(i) t C_D \tag{29}$$

Only solving these two equations, we arrive at the following expressions:

$$\tan\theta(i+1) = \frac{T(i)\sin(\theta(i)) - (dW(i) + dD\cos\theta(i))}{T(i)\cos(\theta(i)) + dD\sin(\theta(i))} \tag{30}$$

$$T(i+1) = \frac{T(i)\cos(\theta(i)) + dD\sin(\theta(i))}{\cos(\theta(i+1))} \tag{31}$$

The tension in the tether at the confluence point can be found using equilibrium analysis. Thus we know $T(1)$. Using Eqs. (27) and (28), we can find the tension $T(i)$ and orientation $\theta(i)$ for all i. Thus we get the entire tether profile and from the profile we can calculate the blowby.

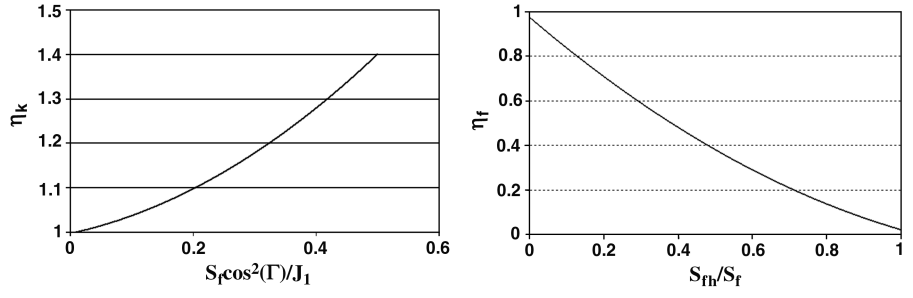

Fig. 5 Hull and fin efficiency factors [10].

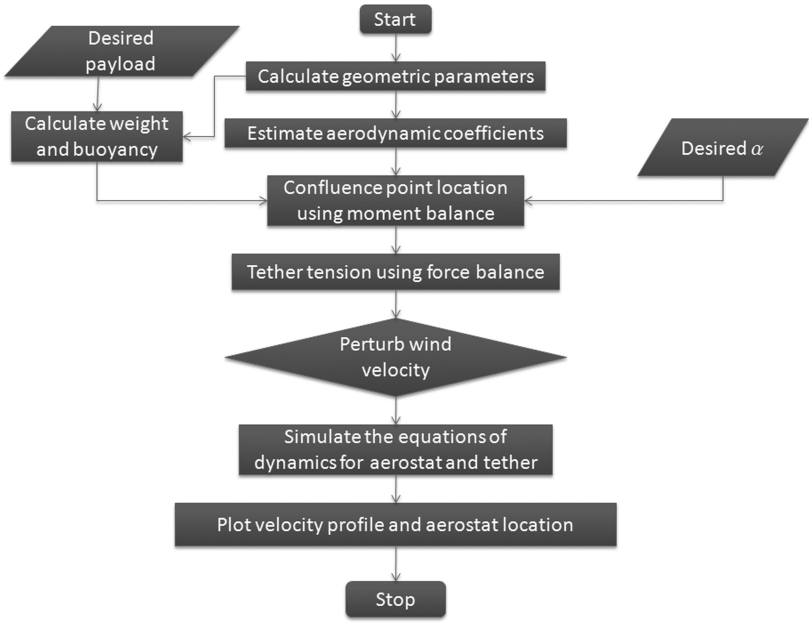

Fig. 7 Flowchart of the program.

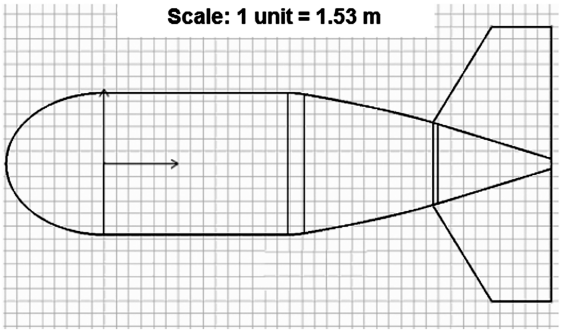

Fig. 8 Approximate profile of TCOM 365Y aerostat [14].

The equilibrium analysis and tether profile estimation completes the static stability analysis of aerostat. The equilibrium state now has to be analyzed for stability. The dynamic simulation model is adopted for stability analysis, details of which are given in the next section.

Table 1 List of assumed parameters

Parameter	Value
α_{eq}	2.5°
β	0
Material density	240 gcm^{-2}
Length of aerostat	67 m
Density of helium	0.1786 kgm^{-3}
Altitude of operation	2000 m
Payload	20% of total weight

Table 2 Calculated and actual values of some geometric coefficients of TCOM 365Y aerostat

Parameter	Computed	Quoted	%error
S_f	0.83322	0.8356	0.285
I_1	0.16679	0.1646	1.33
I_3	−0.18058	−0.1840	1.86
J_1	1.6725	1.6825	0.59
J_2	0.65196	0.6454	1.02
Location of center of buoyancy	0.40683	0.4313	5.67
$C_{L\alpha}$	2.9178	3.0305	3.72

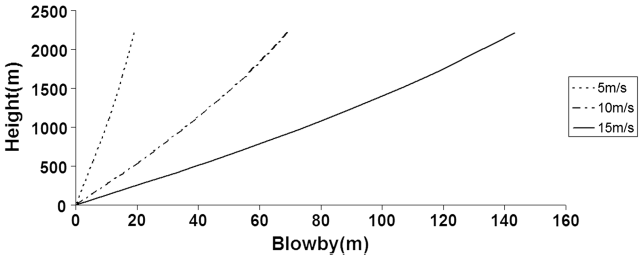

Fig. 9 Tether profiles at equilibrium for various wind speeds.

E. Computer Program for Dynamic Stability Analysis

The dynamic simulation of aerostat's motion under the influence of atmospheric disturbances, and estimation of the shock loads on the tether was carried out using the methodology developed by Jones and Krausman [4]. A MATLAB program was developed by coupling this model to the methodology for equilibrium analysis and tether profile estimation outlined in previous sections. The flowchart of this program is presented in Fig. 7.

The geometric and aerodynamic parameters obtained from this code were compared with those available in literature, and previous studies [14]. The results for the simulation and their possible interpretations are presented in the next section.

V. Results and Comparison

An approximate profile of the TCOM 365Y aerostat is presented in Fig. 8. To analyze the complete aerostat system, a few parameters needed to be assumed. The list of such parameters is provided in Table 1.

On the basis of these assumptions, and the methods described previously, the analysis was performed in a stagewise manner. Firstly, the aerodynamic and geometric parameters were estimated and compared with those available in literature. Table 2 gives a

Table 3 Forces at equilibrium for various wind speeds

Wind velocity, ms^{-1}	5	10	15
Lift, N	533	2138	4820

comparison of actual and calculated values of the geometric parameters. Balancing forces along two mutually perpendicular directions, we obtain the tension force at the confluence point and also the angle along which this tension force is acting. Based on the tension force and its orientation, the tether profile is calculated. Tether profiles, at equilibrium, for different wind speeds are presented in Fig. 9. The magnitudes of various forces acting at equilibrium for various wind speeds is presented in Table 3.

Once equilibrium analysis is completed, the wind is perturbed and velocity and position of the aerostat and tether with time is analyzed.

The apparent and total mass coefficients matrices obtained are as listed in Eqs. (32) and (33), respectively

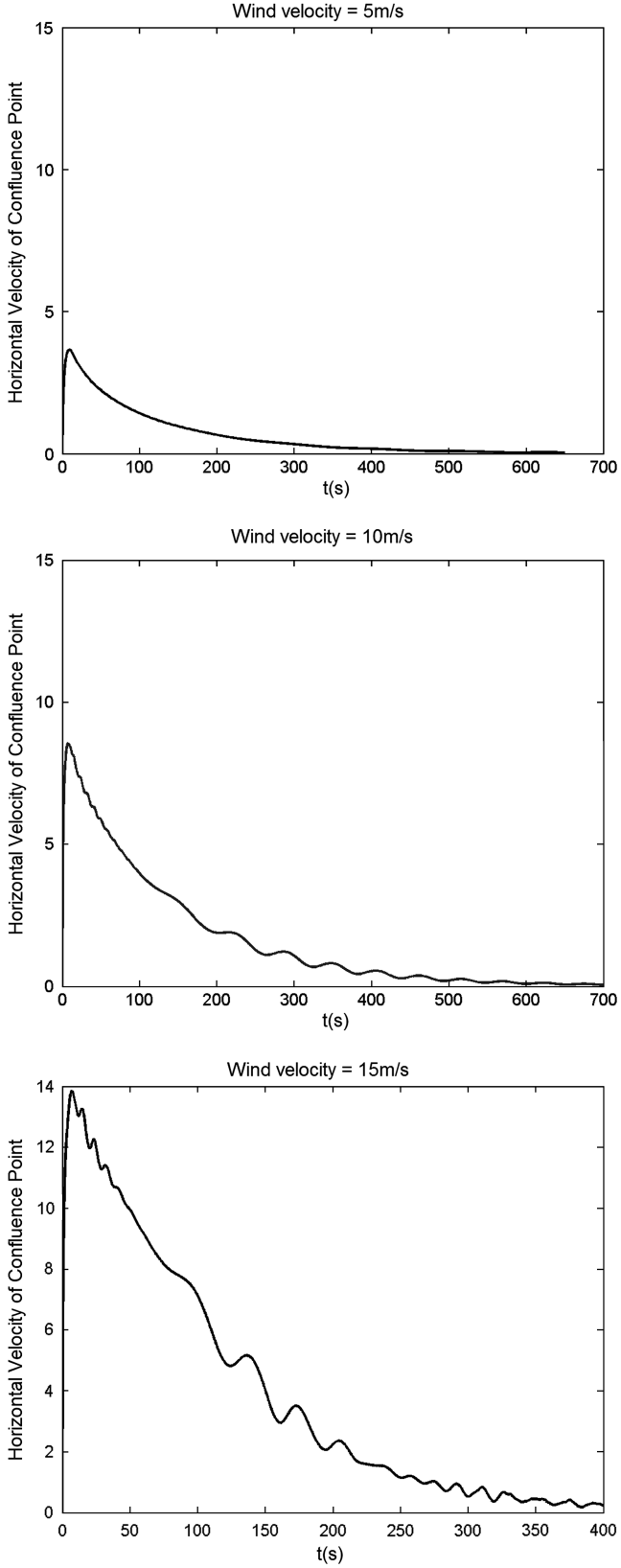

Fig. 10 Horizontal component of velocity of confluence point with time.

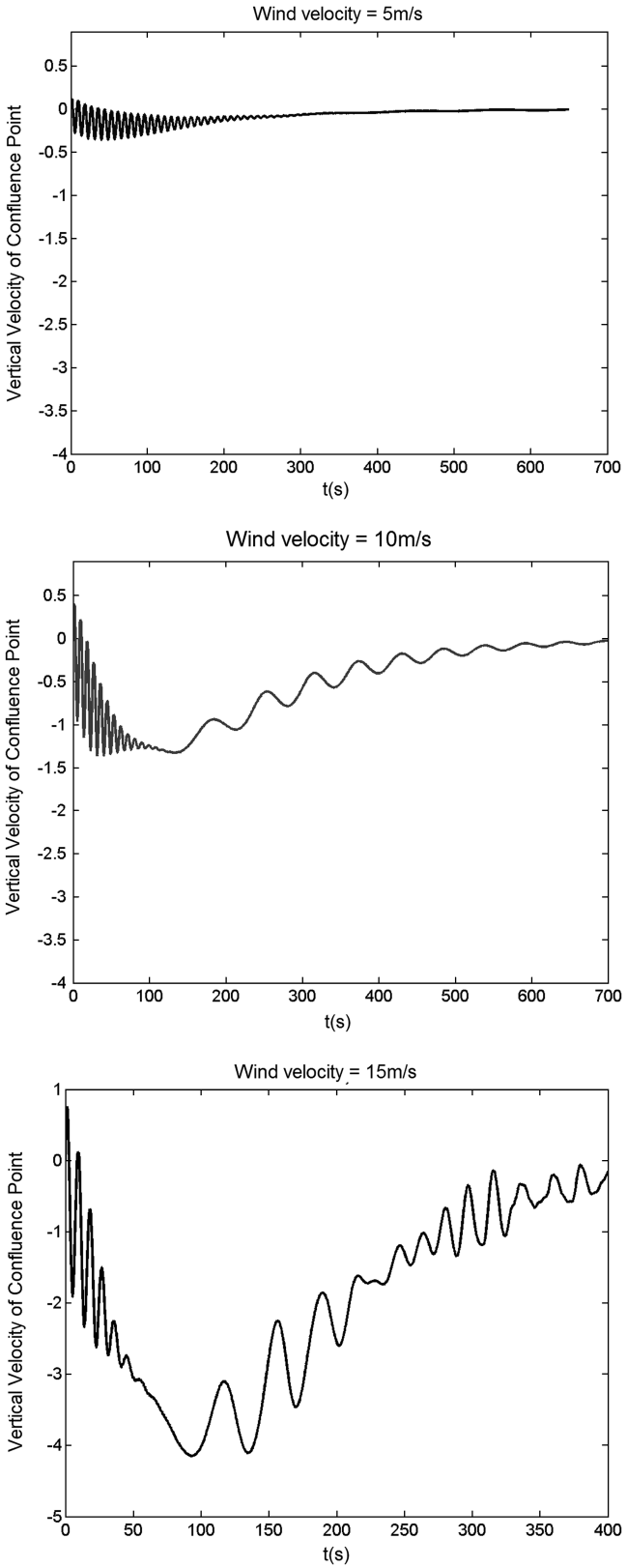

Fig. 11 Vertical component of velocity of confluence point with time.

$$\bar{A}_M = \begin{Bmatrix} 240.3 & 0 & 0 & 0 & 0 & 0 \\ 0 & 623.9 & 0 & 0 & 0 & 0 \\ 0 & 0 & 623.9 & 0 & 0 & 0 \\ 0 & 0 & 0 & 0 & 0 & 0 \\ 0 & 0 & 0 & 0 & 8920.4 & 0 \\ 0 & 0 & 0 & 0 & 0 & 8920.4 \end{Bmatrix} \quad (32)$$

$$\bar{T}_M = \begin{Bmatrix} 344 & 0 & 0 & 0 & 0 & 0 \\ 0 & 344 & 0 & 0 & 0 & 0 \\ 0 & 0 & 344 & 0 & 0 & 0 \\ 0 & 0 & 0 & 26777 & 0 & 0 \\ 0 & 0 & 0 & 0 & 61456 & 0 \\ 0 & 0 & 0 & 0 & 0 & 61456 \end{Bmatrix} \quad (33)$$

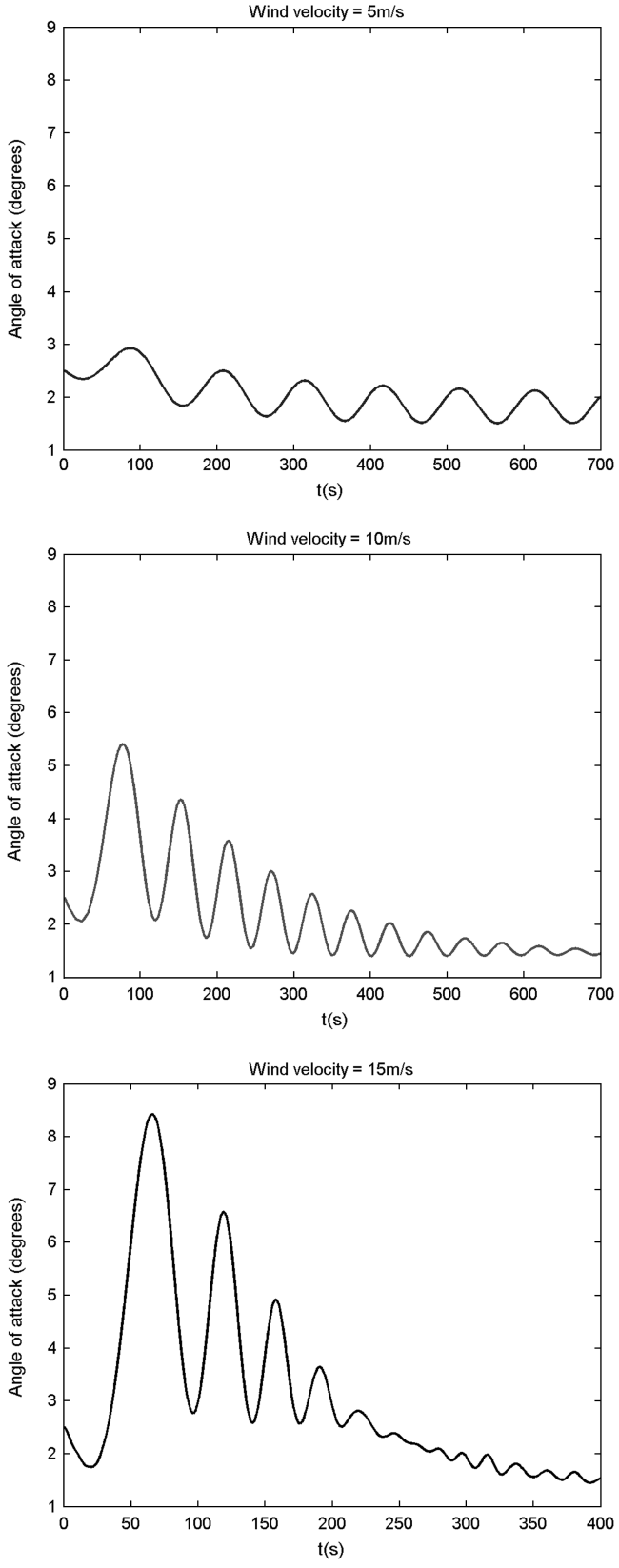

Fig. 12 Variation of angle of attack with time.

Three different steady winds of velocity 5 ms^{-1}, 10 ms^{-1}, and 15 ms^{-1} were applied to perturb the equilibrium state, the results for which are presented here. The equilibrium was established assuming perfectly calm conditions, and then the wind velocity was suddenly increased. The X and Z components of the aerostat velocity are plotted in Figs. 10 and 11 respectively.

As wind velocity is increased, the drag acting on the aerostat as well as the tether increases. Hence the entire system gains a positive velocity in the horizontal direction and starts moving forward. As velocity of the system increases, the relative velocity between system and wind decreases and hence drag starts to decrease. Also, because the aerostat is moving forward, the extension in the tether increases, thereby increasing the tension. A combination of both leads to a steady decrease in the horizontal velocity of the aerostat and after some time it stabilizes to a new equilibrium value as is seen in Fig. 10.

Along the vertical direction, lift increases instantaneously and hence the aerostat has a tendency to rise. The moment the aerostat starts rising, the tension in the tether along the vertical direction increases and hence the tether starts pulling the aerostat down. As the aerostat loses altitude, the tether tension decreases and once again lift comes into the picture and the aerostat again rises. This process repeats and gives rise to the oscillations seen in Fig. 11. The oscillations die out as there is damping in the tether and also lift force decreases with decrease in velocity. The aerostat continues to move until it reaches an equilibrium position at a lower altitude.

The profile for the angle of attack of the aerostat is presented in Fig. 12. The angle of attack undergoes damped oscillations and finally settles to a new equilibrium value. This new equilibrium angle of attack is lower than the previous value as the wind speed has increased. From the plot, it is clear that the oscillations in α die out and the aerostat converges to a new equilibrium angle of attack

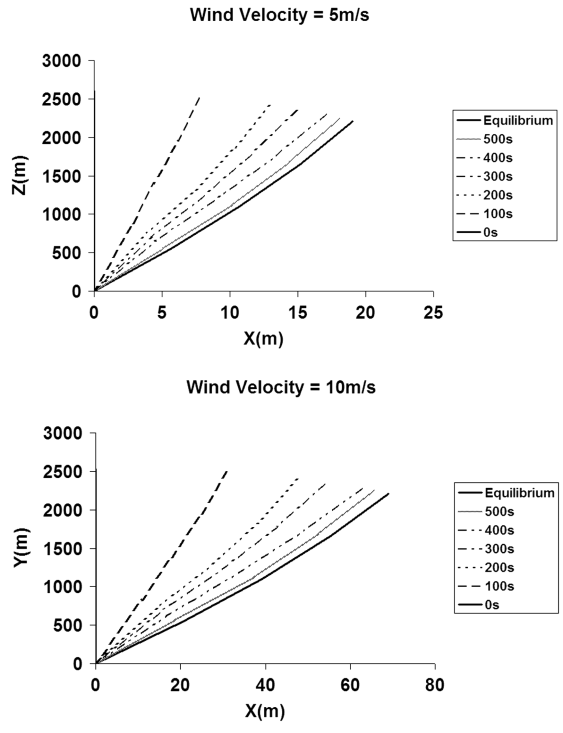

Fig. 13 Profile of the entire system with time.

asymptotically, indicating dynamic stability. The static stability margin, which is given by, $\frac{dC_M}{d\alpha}$ is found out to be -0.246.

A plot for the profile of the entire system with time is presented in Fig. 13. The plot shows the entire system profile at various intervals of time. The topmost point in Fig. 13 refers to the locus of the confluence point in the *X*-*Z* plane with time. This plot gives a true picture of the motion of the entire system in the *X*-*Z* plane.

VI. Conclusions

The geometric and aerodynamic parameters have shown excellent agreement with data available in literature, as is evident from Table 2. The results for the simulation could not be verified as corresponding data was not available. However, the simulations show trends which seem to be correct. The tether profile estimated from static equilibrium analysis for a given wind speed and the tether profile estimated by running simulations for the same wind speed, nearly coincide, as is seen in Fig. 13. We conclude from the graphs that the aerostat is both statically as well as dynamically stable under the assumed wind conditions. The stability of the aerostat under different wind conditions can be analyzed by simply varying the wind velocity. Semi-empirical methods were used in the estimation of the aerodynamic coefficients. Estimation of aerodynamic coefficients could be improved by either using wind-tunnel data or using a better method like CFD analyses, and validated against real life data, where ever available. This would present a clear picture about the accuracy of the results. The effect of the ballonet on stability was neglected due to lack of data. Incorporating a dynamic ballonet model would give much better results. In the development of this model, for ease of calculations, the motion of the aerostat was assumed to be in the *X*-*Z* plane. With minor modifications in the code, and addition of a few equations, it is possible to run simulations for motion in 3-D space. The aerostat response to various wind profiles can be simulated just by varying the wind velocity. Thus its stability can be analyzed for a range of operating conditions.

References

[1] DeLaurier, J. D., "A Stability Analysis for Tethered Aerodynamically Shaped Balloons," *Journal of Aircraft*, Vol. 9, No. 9, 1972, pp. 646–651.

[2] DeLaurier, J. D., "Prediction of Tethered Aerostat Response to Atmospheric Turbulence," *Journal of Aircraft*, Vol. 14, No. 4, 1977, pp. 407–409.
doi:10.2514/3.44602

[3] Jones, S., and DeLaurier, J. D., "Aerodynamic Estimation Techniques for Aerostats and Airships," *Journal of Aircraft*, Vol. 20, No. 2, 1983, pp. 120–126.
doi:10.2514/3.44840

[4] Jones, S., and Krausman, J., "Nonlinear Dynamic Simulation of a Tethered Aerostat," *Journal of Aircraft*, Vol. 19, No. 8, 1982, pp. 679–686.
doi:10.2514/3.57449

[5] Jones, S., and Schroeder, L., "Nonlinear Dynamic Simulation of a Tethered Aerostat: A Fidelity Study," *Journal of Aircraft*, Vol. 38, No. 1, 2001, pp. 64–68.
doi:10.2514/2.2735

[6] Lambert, C., and Nahon, M., "Stability Analysis of a Tethered Aerostat," *Journal of Aircraft*, Vol. 40, No. 4, 2003, pp. 705–715.
doi:10.2514/2.3149

[7] Stanney, K. A., and Rahn, C. D., "Response of a Tethered Aerostat to Simulated Turbulence," *Communications in Nonlinear Science and Numerical Simulation*, Elsevier, New York, Vol. 11, 2006, pp. 759–776.

[8] Rawat, P., "Nonlinear Analysis of Aerostat Behavior," *7th AIAA Aviation Technology, Integration and Operations Conference & 17th Lighter-Than-Air Systems Technology Conference*, AIAA, Reston, VA, 2007.

[9] Panda, G., and Krishnamurthy, M., "Equilibrium Analysis of a Tethered Aerostat," *Project Document FE 9802, Flight Experiments Division*, National Aerospace Lab., Bangalore, India, Nov. 1998.

[10] Gill, P., Malik, S., and Pant, R., "Estimation of Aerodynamic Characteristics of Un-Symmetrically Finned Bodies of Revolution," *28th National Conference on Fluid Mechanics and Fluid Power*, National Society of Fluid Mechanics and Fluid Power, Chandigarh, India, 2001.

[11] Raymer, D. P., *Aircraft Design: A Conceptual Approach*, AIAA Education Series, AIAA, Reston, VA, 1989.

[12] Munk, M., "Aerodynamics of airships," *Aerodynamic Theory VI* edited by W. F. Durand, Springer, New York, 1936, pp. 32–48.

[13] Hoerner, S. F., *Fluid Dynamic Drag*, S. F. Hoerner, Brick Town, NJ, 1975.

[14] Vijayram, C., and Pant, R., "Multidisciplinary Shape Optimization of Aerostat Envelopes," *7th AIAA Aviation Technology, Integration and Operations Conference & 17th Lighter-Than-Air Systems Technology Conference*, AIAA, Reston, VA, 2007.

[15] Gupta, S., "Lighter-Than-Air Technology of ADRDE: An Overview," *Continuing Education Program on Design and Testing of Aerostat Systems*, Aerial Delivery Research and Development Establishment, Agra, India, 2007, pp. 1–25.

[16] Wardlaw, A. B., *High Angle-of-Attack Missile Aerodynamics*, AGARD Lecture Series, No. 98, Technical Editing and Reproduction Ltd., London, Feb. 1979.